Journal of Materials Chemistry B

Accepted Manuscript

ROYAL SOCIETY OF CHEMISTRY

www.rsc.org/materialsB

Controlling Whole Blood Activation and Resultant Clot Properties by Carboxyl and Alkyl Functional Groups on Material Surfaces: A Possible Therapeutic Approach for Enhancing Bone Healing

Hoi Ting Shiu, Ben Goss, Cameron Lutton, Ross Crawford, Yin Xiao**

Running title: Blood clot and bone regeneration

Institute of Health and Biomedical Innovation, Queensland University of Technology, Brisbane, Queensland, QLD 4059, Australia

Keywords: biomaterials, coagulation, bone, growth factor, surface chemistry.

**Corresponding author*
Prof. Yin Xiao and Dr Ben Goss
Bone and Tissue Engineering, Institute of Health and Biomedical Innovation, Queensland University of Technology, Kelvin Grove Campus, Brisbane, Qld 4059 Australia
Tel: +61 7 3138 6240
Fax: +61 7 3138 6030

E-mail: yin.xiao@qut.edu.au, bgoss@nuvasive.com

Abstract

Most research virtually ignores the important role of a blood clot in supporting bone healing. In this study, we investigated the effects of surface functional groups carboxyl and alkyl on whole blood coagulation, complement activation and blood clot formation. We synthesised and tested a series of materials with different ratios of carboxyl (–COOH) and alkyl ($–CH_3$, $–CH_2CH_3$ and $–(CH_2)_3CH_3$) groups. We found that surfaces with –COOH/$–(CH_2)_3CH_3$ induced a faster coagulation activation than those with –COOH/$–CH_3$ and $–CH_2CH_3$, regardless of the –COOH ratios. An increase in –COOH ratios on –COOH/$–CH_3$ and $–CH_2CH_3$ surfaces decreased the rate of coagulation activation. The pattern of complement activation was entirely similar to that of surface-induced coagulation. All material coated surfaces resulted in clots with thicker fibrin at denser network at the clot/material interface and a significantly slower initial fibrinolysis when compared to uncoated glass surfaces. The amounts of platelet-derived growth factor-AB (PDGF-AB) and transforming growth factor-β (TGF-β1) released from an intact clot were higher than a lysed clot. The release of PDGF-AB was found to be correlated with the fibrin density. This study demonstrated that surface chemistry can significantly influence the activation of blood coagulation and complement system, resultant clot structure, susceptibility to fibrinolysis as well as release of growth factors, which are important factors determining bone healing process.

1. Introduction

Severe bone damage requires bone tissue engineering, which aims to provide three key elements for bone repair: the scaffolding for osteoconduction, growth factors for osteoinduction, and progenitor cells for osteogenesis[1, 2]. To date, no engineered material outperforms autograft in bone-forming ability[3]. Therefore, further understanding of how biomaterials used for scaffolds interact with host tissue and affect bone formation will be helpful for the improvement of tissue engineering[4].

Platelet-rich plasma (PRP) which has been applied in clinical dentistry for over a decade provides an insight into the microenvironment required. PRP is a fraction of plasma with a high concentration of platelets and serves as an autologous source of growth factors[5]. Studies have shown that formation of PRP gels to bone grafts or biomaterials increases the rate of bone formation and bone density[6], possibly due to increased concentrations of growth factors derived from platelets, and adhesive binding of graft particles by the fibrin network[7]. However, other groups have shown conflicting results when PRP clots were prepared with different platelet numbers and thrombin concentration[8]. Thus, these findings imply that the effect of clots on bone healing depends on how the clots are formed.

During clot formation, thrombin concentration is known to affect fibrin thickness and density[9, 10]. Whilst abnormal changes in clot structure have been shown to influence the viscoelastic properties [11, 12] and lysis rate of clots[13], leading to pathological conditions such as cardiovascular thrombosis and bleeding disorders[14, 15]. Indeed, dental implant has long demonstrated that a peri-implant clot plays an important role in endosseous healing[16]. Chemokines released from entrapped blood cells and fibrin network of the peri-implant have been shown to support continuous recruitment and migration of osteogenic cells, resulting in a direct bone formation on the implant surfaces[17]. Thus the ability to control the properties of a blood clot formed on the implant appears as a critical design parameter which would influence cellular response and tissue ingrowth in bone healing.

Upon implantation, activation of blood coagulation occurs rapidly when whole blood makes contact with the surface of a synthetic implant. The adsorption of plasma proteins is believed to initiate platelet

reactions and coagulation activation, leading to the generation of thrombin and fibrin, and ultimately formation of a blood clot on the implant surface[18]. Despite this phenomenon is generally being aware of, few studies have explored early blood-endosseous implant interactions and resulting blood clot formation, even if these events occur prior to bone regeneration. A peri-implant clot may be beneficial for bone repair when the clot has biological and structural properties similar to those of the haematoma formed on injured bone during native healing. On the other hand, an important concern of the blood-biomaterial interactions is the activation of the complement pathway and its potential to initiate chronic inflammation or foreign body reaction (FBR). These adverse reactions may cause the deterioration of the implanted biomaterial and secondary injury to surrounding tissue.

To minimise immunogenic and improve anti-thromboticity of blood contacting devices, many research has been focused on modifying surface chemistry of biomaterials, particularly the species and density of surface chemical functionalities. Alkythiols or alkysilanes self-assembled monolayers (SAMs) are often used as a flat surface model. SAMs presenting 47% –COOH/53%–CH_3 chemical functionalities have been shown to increase coagulation activation resulting in a strong fibrin fibre deposition, whereas decrease leukocyte accumulation and complement initiation when compared with pure –COOH and –CH_3. SAMs [19]. In addition, it has been found that poly (alkyl methacrylates) with different chain length of alkyl groups provide further level to regulate these blood-biomaterial interactions [20]. Coincidently, poly (methyl methacrylate) (PMMA) is widely used as a bone cement, dental fillings and intraocular lenses [21]. Polymers containing ethyl methacrylate (EMA) or butyl methacrylate (BMA) have also been shown to modulate chondrocyte and osteoblast attachment, and induce angiogenesis, respectively [22, 23]. Specifically, copolymers composed of methyl methacrylate (MMA) and acrylic acid (AA), which presents –COOH groups, has been confirmed to be non-toxic both *in vitro* and *in vivo* and served as a drug delivery system [24]. Unlike SAMs on gold substrates which is not clinically feasible, such copolymers of alkly methacrylate and acrylic acid may provide a coating to form the basis of three-dimensional material surfaces in developing a prothrombogenic and immunocompatible coating for synthetic bone implants.

Given that most current approaches in bone tissue engineering focus solely on the replacement of viable cells, growth factors, and functional structure using engineered scaffolds, it often overlooks the importance of blood clot formation around scaffolds in controlling bone healing. In this study, we hypothesised that the bone-inducing ability of a biomaterial may be improved by controlling the blood-biomaterial interactions and forming a desirable peri-implant blood clot with appropriate properties. We developed an *in vitro* incubation vial where the inner surface was coated with materials of acrylic acid (AA) and methyl (MMA), ethyl (EMA), or butyl methacrylates (BMA) at varied ratios. The effect of surface functional groups and their relative ratios on coagulation and complement activation as well as alterations in resultant clot structure, susceptibility to fibrinolysis and the release of platelet-derived growth factor (PDGF-AB) and transforming growth factor-β1 (TGF-β1) were investigated.

2. Materials and Methods

2.1. Synthesis of materials: Acrylic acid and alkyl methacrylate were reacted via free-radical polymerisation using benzoyl peroxide (BPO) as an initiator. Three types of alkyl methacrylates were employed: methyl methacrylates (MMA), ethyl methacrylates (EMA) and butyl methacrylates (BMA). The monomer solutions were added at molar ratios (AA: alkyl methacrylate; 45, 55 or 65 %) in a glass vial containing 0.5% of BPO. The solutions were deoxygenated by bubbling argon gas with a syringe through the septum caps on the vials. The vials were then incubated in an oil bath with increasing temperatures (45˚C, 55˚C, 65˚C, 75˚C, 85˚C) for 1 h intervals and at 90 ˚C and 100˚C for 20 min intervals.

2.2 Preparation of surface coatings: The impact of the surface functionalities and their relative ratios on blood responses was studied by incubation vials with surface coatings. The materials prepared as described above were dissolved in acetone to give a 5 % (w/v) solution. The solutions were coated on the internal surface of glass vials (4 mL, 15x45 mm; Waters, Australia) by a solvent-evaporation technique[25]. Solutions of 1.5 mL were added to the vials and dried in an oven at 50 ˚C until complete evaporation of acetone. The procedure was repeated three times to ensure full

coverage on the glass surfaces. After drying, the coated vials were capped at room temperature until used.

For water contact angle measurement, glass coverslips (No. 1, diameter 13 mm, ProSciTech, Australia) were used to provide a flat surface. Coverslips were placed at the bottom of glass vials before the addition of solution and drying step. Uncoated glass vials or coverslips were used as controls.

2.3 Characterisation of surface: To analyse the surface properties of the coating, the coated vials or coverslips were cut manually. The functionalization of coatings was analysed by X-ray photoelectron spectroscopy (XPS) (Centre for Microscopy and Microanalysis, University of Queensland). A spectrometer (Axis ULTRA Kratos Analytical, Shimadzu, UK) equipped with a monochromatic Al Kα X-rays (1486.6eV) was operated at 150 W and incident at 45 ° to the sample surface. Photoelectrons emitted from the surface were collected at a take-off angle of theta 90 ° with a 165 mm hemispherical electron energy analyser. Elements present in the surface were identified by survey scans taken at pass energy of 160 eV and at resolution of 1.0 eV. These scans recorded binding energies of the photoelectrons ranging from 0 - 1200 eV. Multiplex scans at pass energy of 20 eV and at a higher resolution of 0.05 eV were also performed to determine the chemical states of carbon atoms. The base pressure in the chamber was 1.0×10^{-8} torr during analysis.

The carbon 1s (C1s) high resolution spectra were processed to determine the relative oxidation states of carbon atoms. Curve fitting of the spectra was performed using the Casa XPS software (version 2.3.14) and a linear baseline with Kratos library Relative Sensitivity Factors (RSFs). The binding energies that are indicated by peaks in spectra were referenced to the C1s aliphatic carbon peak at 285.0 eV. This corrected the effect of surface charging during analysis on shifting the peak positions. Peak areas were normalised and adjusted to obtain a full width at half maximum between 0.9 and 1.1 eV. By determining the area ratios of carbonyl (C-O) component derived from methacrylate monomer, and carboxyl (O-C=O) component derived from both types of comonomers, the compositions of corresponding surface functionalities were obtained. Average data were collected from three

measurements of each surface. Surface hydrophobicity of coatings were assessed by measuring advancing water contact angle using a FTÅ 200 system (First Ten Ångstroms, Poly-Instruments Pty. Ltd., Australia). Drop shape analysis software (Fta32 version 2.0) was used and data were the average of at least six regions of each surface. Surface morphology of coatings on glass vials were examined by scanning electron microscopy (SEM) with a Quanta 200 scanning electron microscope (FEI, USA) (at a magnification of 25000 x). The roughness of surface coating was measured by atomic force microscopy (AFM) using a Solver P47 Pro scanning probe microscope (NT-MDT Co., Russia). Sample surfaces were scanned in contact mode (constant force) with a golden silicon probe (CSG 11 No. 2 rectangular, NT-MDT Co.). NT-MDT Image Analysis software (version 2.2.0) was used to obtain mean of at least six regions of each surface.

2.4 Blood sampling and in vitro incubation: Whole blood was collected from a healthy volunteer who was not on any medication for at least 10 days and with no history of coagulation disorders. Venipuncture was performed by a phlebotomist. Venous blood was drawn into syringes with a 19-gauge needle and immediately transferred (1.5 mL) to the vials and incubated at 37 ˚C. After the desired incubation time, all blood contents in the vials were collected and processed for following experiments. This procedure was approved by the Human Ethics Committee of the Queensland University of Technology. Informed consent was also obtained from donor prior to blood collection.

2.5 In vitro coagulation activation: Activation of the coagulation cascade leads to the conversion of prothrombin into active thrombin, a process accompanied with the production of prothrombin fragment 1+2 (F1+2). To assess *in vitro* coagulation activation on the coated surfaces, prothrombin F1+2 was analysed using an enzyme-linked immunosorbent assay (ELISA, Enzygnost® F1+2; Dade Behring Marburg GmbH, Germany). Based on our preliminary studies, the coagulation was analysed after 30 min of whole blood incubation as the formation of F1+2 demonstrated well established differences among surfaces. Serum was isolated by transferring samples from incubation vials to microcentrifuge tubes containing tri-sodium citrate (0.11 mol/L) (one part of tri-sodium citrate with 9 parts of blood sample) and centrifuged according to the manufacturer's protocols. Plasma levels of F1+2 serve as a

baseline and were obtained by centrifuging blood in Vacuette® test tubes containing sodium citrate (3.5 mL blue capped, Greiner Labortechnik, Austria). All data were obtained from 6 replicates of each surface.

2.6 In vitro complement activation: Initiation of the complement system leads to the formation of a common end product C5a convertase, which cleaves complement protein C5 to C5a. C5a is rapidly transformed to C5a-des Arginine (C5a-desArg) by endogenous carboxypeptidase N enzyme in plasma or serum. To determine the extent of complement activation on material-coated surfaces, serum C5a-desArg was quantified with Human C5a ELISA Kit II (OptEIA^{TM}; BD Bioscience, USA). Serum collected from blood samples after 2 h incubation was analysed as the formation of C5a-desArg were detectable and more pronounced based on our preliminary study, which also agrees with earlier findings[26]. The sandwich ELISA assay was performed as manufacturer's instruction. A background level of complement activation monitored as plasma level of C5a-desArg was obtained by centrifuging blood in Vacuette® test tubes containing EDTA (4.0 mL purple capped, Greiner Labortechnik, Austria). All data were obtained from 6 replicates of each surface.

2.7 Characterisation of clots formed on material-coated surfaces

Examination of clot structure: To study whether clot architecture was altered by surfaces presenting various compositions of functional groups, the clots formed in incubation vials were examined by SEM. After 2 h incubation, the clots were fixed with 4% paraformaldehyde (pH 7.4) at 4 ˚C overnight. The clots were washed twice with phosphate buffered saline (PBS, pH 7.4) for 30 min, and dehydrated in grades of ethanol (50 %, 70 % and 100 %) for 1 h per grade. A longitudinal cut was performed on the clots to allow examination of the ultrastructures at clot/material interface and the centre of the clot. Following dehydration, the clots were processed through 100 % amyl acetate twice of 15 min intervals and dried in a CO_2 critical point dryer. The clots were then mounted, gold-coated and examined with the SEM microscope. Representative images were captured.

2.8 Fibrin thickness measurement: The effect of material surfaces on fibrin formation in the clots was assessed by measuring the diameter of fibrin strand from SEM images at 5000 x magnification. The

measurement was performed using Image J software (version 1.43). A transverse line was drawn perpendicular to long axis of the fibre with clearly defined margins. The pixel value was related to that obtained for the scale bar on the image. At least forty different fibrin strands were measured at random fields approximate 50 μm away from the edge of clot and in the centre of the clot. A minimum of two images were analysed for each sample. The diameter of individual fibrin of each sample was reported as an average for all fibres measured.

2.9 Fibrin density measurement: Quantitative fibrin network analysis was performed using Image J software (version 1.43) using a modified method of Undas *et al*.[27]. A 64-field grid was generated to cover each SEM image and at least twenty fields were selected randomly at the edge and in the centre of the clots. The density of fibrin fibre was determined by counting the number of fibres per field (40 μm^2) and the mean value was presented.

2.10 Clot lysis assay: Clot lysis strongly correlates with fibrin thickness and density. The effect of material surfaces on overall clot degradability was investigated and its relationship to the fibrin architecture as determined above was studied. Clot lysis was evaluated by the generation of fibrin degradation product (D-dimer) when the cross-linked clots were digested by fibrinolytic enzymes *in vitro*.

A suspended clot system modified from the protocols of Collet *et al*. [14]was used in this study. Whole blood was incubated (1.5 mL) in the vials for 2 h at 37 ˚C to allow complete clot formation and retraction. The clots were removed carefully from the vials and suspended in 3 mL of PBS containing human plasminogen (Glu-plasminogen, 5.4 μg/mL final concentration; American Diagnostica Inc., USA) [28]. Lysis of the clot was induced by adding recombinant tissue-type plasminogen activator (tPA, 0.25 μg/mL final concentration; American Diagnostica Inc., USA) at 37 ˚C with gentle agitation. This concentration of tPA was determined as the lowest one able to induce clot lysis as determined in preliminary study (data not shown). Aliquots of 300 μL were removed at timed intervals and centrifuged at 1000 g for 3 min. The supernatants were stored at -70 ˚C before analysis. The same volume of PBS was supplemented after samplings. The extent of clot lysis was monitored by measuring

the amounts of D-dimer released from the clots using IMUCLONE® D-Dimer ELISA (American Diagnostica Inc., USA). Clots that were suspended in PBS only were used as control of spontaneous fibrinolysis. Weight loss of clots during lysis was also traced during the experiments. All data was obtained from triplicate of clots formed on each surface.

2.11 Quantification of growth factors: The release of platelet-derived growth factor-AB (PDGF-AB) and transforming growth factor-β1 (TGF-β1) during both clot formation and clot lysis was assayed by ELISA. After 2 h incubation, supernatant serum above the clots was collected and the clots were directly subject to clot lysis as described previously. Supernatant serum and buffer aliquots collected at varied intervals were centrifuged for 15 min at 1000 g and assayed according to the manufacturer's instructions. All Quantikine® ELISA kits were purchased from R&D Systems (Minnesota, USA) and the sandwich ELISA assay was performed. To detect the circulating levels of growth factors, platelet-poor plasma was prepared by centrifuging blood in Vacuette® test tubes containing EDTA for 15 min at 1000 g and subsequently for 10 min at 10,000g (4.0 mL purple capped, Greiner Labortechnik, Austria). All data were obtained from triplicates of clots formed on each surface.

2.12 Statistical analysis: Data from the experiments were expressed as the mean values ± standard deviation. Analysis was performed using SigmaPlot (version 11.0; Systat software Inc). The data from control and test surface were compared using the Student's *t*-test. For multiple comparisons, one-way analysis of variance (ANOVA) was used with the Holm-Sidak's test. The significance level was set at $p \leq 0.05$.

3. Results

3.1 Synthesis and characterisation of biomaterials coated on the surface of vials – Spectra, hydrophobicity and roughness

The surfaces containing materials of AA and MMA/EMA/BMA are named according to the mole fractions of AA (45, 55, 65%), for instance 45% AA/ 55% MMA as 45 MMA etc. Materials of a single component (i.e homopolymers: PAA, PMMA, PEMA, and PBMA) served as references.

Materials including 45BMA (containing 25% –COOH); 55MMA, 55EMA & 55BMA (containing 33% –COOH) and 65MMA, 65EMA & 65BMA (containing 40% –COOH) were used in this study. The synthesised materials were coated into vials and characterised to ensure the correct ratios of carboxyl and alkyl groups were achieved. Spectra by X-ray photoelectron spectroscopy (XPS) of surfaces were shown in **Figure 1a-d**. C1s spectra demonstrated alkyl methacrylates differ from acrylic acid by a prominent peak corresponding to carbon component C-O (286.8 eV), whereas both comonomers showed three common components: C-C (285.0 eV), C-COO (285.7 eV), and O-C=O (289.1 eV) (**Figure1e-g**). The relative compositions of C-O and O-C=O on surface coatings were measured from the peak areas. The surface ratios of –COOH/–CH_3, –CH_2CH_3 or $(CH_2)_3CH_3$ are summarised in **Table 1**. As clearly demonstrated by BMA surfaces, the surface coatings became increasingly richer in –COOH group (i.e. increased X_{COOH} coating) with the increase in the AA monomer feed (i.e. increased X_{COOH} material). Interestingly, X_{COOH} material of 0.45 and 0.55 at MMA and EMA surfaces showed similar X_{COOH} coating concentrations (i.e. 0.32 – 0.34). Also, X_{COOH} coating at MMA, EMA and BMA surfaces were found to be comparable at X_{COOH} material of 0.55 (0.33, 0.32 &0.34 respectively), and of 0.65 (0.41, 0. 39 & 0.41 respectively).

The advancing water contact angle of an uncoated glass substrate was 54.1 ± 4.2 º. With addition of a coating, the values increased to 77.6 ± 3.1 º, 82.9 ± 1.0 º and 91.8 ± 4.4 º for PMMA, PEMA and PBMA, respectively (**Table 2**). These results were in agreement with published data [29]. The contact angle values of homopolymer-derived coatings increased significantly in the order: –CH_3 < –CH_2CH_3 < –$(CH_2)_3CH_3$, suggesting the surface hydrophobicity increased with the alkyl chain length ($p \leq 0.001$). Similarly, at the same –COOH ratios, a significantly higher contact angle was observed on surfaces with –$(CH_2)_3CH_3$ groups compared to those with –CH_3 and –CH_2CH_3 groups (i.e. At an average 33% –COOH from X_{COOH} material of 0.55, p=0.005; At an average 40% –COOH from X_{COOH} material of 0.65, $p \leq 0.001$). On the other hand, an increase in –COOH ratio (0% to 41%) on –COOH/–$(CH_2)_3CH_3$ surfaces led to a decrease in contact angle. This indicated that surface hydrophobicity was strongly influenced by the functional groups and their ratios.

Scanning electron microscopy (SEM) and atomic force microscopy (AFM) showed that all coated surfaces exhibited as smooth as the uncoated surfaces (data not shown).

3.2 Effects on coagulation responses

The serum level of prothrombin F1+2 after 30 min incubation was shown in **Figure 2a**. All material-coated surfaces had higher levels than the plasma (0.014 ± 0.0007 %, i.e. 0.06 ± 0.003 nmol/L) but lower levels compared to the uncoated glass surfaces ($p \leq 0.001$). In general, BMA surfaces induced significantly higher F1+2 level than MMA and EMA surfaces, regardless of the –COOH ratios ($p \leq 0.001$). Amongst BMA surfaces with various –COOH ratios, 55BMA had a slightly higher F1+2 level compared to 45BMA and 65BMA but no significant difference was detected ($p = 0.305$). Among 55MMA, 55EMA & 55BMA surfaces with approximately 33% –COOH, 55BMA showed the highest F1+2 level whereas 55EMA showed the lowest level ($p \leq 0.001$). A similar effect of alkyl groups on coagulation activation was also found on surfaces with a higher content of –COOH (i.e. 40% on 65MMA, 65EMA & 65BMA) ($p \leq 0.001$). In contrast to BMA surfaces, an increase in –COOH ratio on MMA and EMA surfaces reduced F1+2 level significantly ($p \leq 0.001$).

3.3 Effect on complement response

The serum level of C5a-desArg after 2 h incubation was shown in **Figure 2b**. All material-coated surfaces had dramatically reduced level compared with the uncoated glass surfaces, though expectedly higher than the plasma level (6 ± 1%, i.e. 7 ± 1 ng/mL) ($p \leq 0.001$). Similar to the trends observed for coagulation activation, BMA surfaces generally had higher C5a-desArg level than MMA and EMA surfaces ($p \leq 0.001$). Among BMA surfaces, 55BMA had a significantly lower level than 45BMA and 65BMA ($p \leq 0.001$). No difference was found between the latter two surfaces.

For surfaces with approximately 33% –COOH (55MMA, 55EMA & 55BMA), and 40% –COOH (65MMA, 65EMA & 65BMA), a lower C5a-desArg level was found on EMA surface for both percentages ($p \leq 0.001$). An increase in –COOH ratio on MMA and EMA surfaces also further reduced C5a-desArg level ($p = 0.036$; $p = 0.04$, respectively). The lowest C5a-desArg level among all coated surfaces was on the 65EMA surface. Overall, the extent of complement activation was significantly

elevated in the presence of $–(CH_2)_3CH_3$ groups, but reduced in the presence of $–CH_2CH_3$ groups. Increasing –COOH ratio on the surfaces with $–CH_3$ and $–CH_2CH_3$ groups further reduced complement response.

3.4 Effect on clot morphology and structure

The effect of various ratios of surface –COOH groups on clot structure was shown by 45BMA, 55BMA and 65BMA. As shown in **Figure 3a-d**, the edge of clots formed on BMA surfaces showed thicker fibrin fibers at a denser network. In contrast, the edge of clots formed on uncoated glass surfaces showed thinner fibers at a loose network . The fibrin at the edge of clots on glass surfaces were significantly smaller in diameter (**Figure 3i**) and lower in density (**Figure 3k**) than those of BMA surfaces ($p \leq 0.001$). Among BMA surfaces, the fibrin diameter at the edge of clots was significantly smaller on 55BMA, while the fibrin density was significantly lower on 45BMA ($p \leq 0.001$). No difference in fibrin density at the edge was found between 55BMA and 65BMA ($p = 0.237$). In addition, fibrin architecture was found to change dramatically from the edge to the centre of the clot (**Figure 3e-h**). In the centre of clots, the fibrin of all surfaces except 45BMA increased in diameter (**Figure 3j**), while the densities of all surfaces decreased approximately 3 to 5 times ($p \leq 0.001$) (**Figure 3l**).45BMA produced significantly thinner fibres ($p \leq 0.05$) at higher density ($p \leq 0.001$) than all other surfaces. Overall variation of the –COOH ratio on $–(CH_2)_3CH_3$ bearing surfaces led to significant changes in the fibrin thickness and network density.

The effect of surface alkyl groups on clot structures was illustrated by 65MMA, 65EMA & 65BMA. The clots formed on surfaces with approximately 40% –COOH (65MMA, 65EMA & 65BMA) and uncoated glass surfaces were observed in Figure **4a-d**. Compared to the uncoated glass surfaces, the fibrin fibres at the edge of clots formed on 65MMA, 65EMA and 65BMA were significantly larger in diameter and higher in density ($p \leq 0.001$) (**Figure 4i, k**). Among 65MMA, 65EMA and 65BMA surfaces, the fibrin diameter at the edge of the clots of 65BMA was significantly larger than the others ($p \leq 0.001$). No difference was found between those of 65MMA

and 65EMA ($p = 0.287$). Moreover, the fibrin density was significantly higher on 65MMA while lower on 65EMA ($p \leq 0.001$).

Compared to the fibres at the edge, the fibres at the centre of the clots on all surfaces except 65EMA increased in diameter (**Figure 4j**), and the fibrin densities of all surfaces decreased approximately 5 times ($p \leq 0.001$) (**Figure 4l**). While the fibrin diameter of 65EMA was significantly smaller than those of 65MMA and 65BMA ($p \leq 0.001$), no significant differences were found between the latter ($p = 0.105$). For the fibrin density at the centre of the clots, it was significantly higher on 65MMA than all the others ($p \leq 0.001$). Although the mean fibrin densities of 65EMA and 65BMA were not significant different, a similar trend in fibrin density was observed at the edge and at the centre of clots formed on 65MMA, 65EMA and 65BMA.

3.5 Effect on fibrinolysis

To evaluate the effect of various ratios of surface –COOH groups on fibrinolysis, D-dimer levels from the clots of 45BMA, 55BMA and 65BMA were compared. After 1 h of lysis, all BMA surfaces revealed significant decrease D-dimer levels compared to uncoated glass surfaces (Figure 5a), suggesting the clots of BMA surfaces initially underwent a slower rate of fibrinolysis. In addition, 55BMA led to a faster fibrinolysis whereas 65BMA led to a slower rate. Consistent with 1 h of lysis, the mean D-dimer level of 55BMA progressively increased compared to the other BMA surfaces over the rest of lysis period, with a significant difference detected after 8 h of lysis ($p \leq 0.05$) (Figure 5c). Taken together, BMA surfaces displayed a delayed onset of fibrinolysis during the first hour of lysis compared to the uncoated glass surfaces.

To evaluate the effect of surface alkyl groups on fibrinolysis, the clots of surfaces exhibiting 40% –COOH (65MMA, 65EMA & 65BMA) were compared. In accordance to BMA surfaces, 65MMA, 65EMA and 65BMA surfaces showed a significant slower fibrinolysis than uncoated glass surfaces after 1 h of lysis (Figure 5b). Among the coated surfaces, 65MMA showed a significantly slower fibrinolysis whereas 65EMA showed a faster rate. No significant differences were found for the rest of the lysis period (Figure 5d).

As evident from uncoated glass surfaces (Figure 5e), the control clots subjected to PBS buffer only showed a negligible amount of D-dimer as to the plasma level (0.06 ± 0.005 μg/mL to 2.8 ± 0.287 μg/mL from 1 h to 24 h after lysis) when compared to the clots exposed to tPA and plasminogen in PBS buffer. This suggested that the spontaneous fibrinolysis was not profound and our suspended clot system supplemented with fibrinolytic enzymes was feasible for assaying clot lysis.

3.6 Effect on PDGF-AB and TGF-β1 release

The release of PDGF-AB and TGF- β1 in supernatant serum after clot formation on 65MMA, 65EMA and 65BMA surfaces was shown in **Figure 6**. Significantly elevated PDGF-AB (**Figure 6a**) and TGF- β1 (**Figure 6b**) levels were found on all surfaces compared to plasma baseline (308 ± 49 pg/mL for PDGF-AB and 1021 ± 31 pg/mL for TGF-β1). This confirmed the growth factors are released upon clot formation. Among 65MMA, 65EMA & 65BMA surfaces, 65MMA showed a significantly higher PDGF-AB level compared to 65EMA ($p \leq 0.05$). For TGF-β1, however, we found no significant differences among coated and uncoated surfaces.

The release of growth factors in the buffer during clot lysis was also assessed. The degrading clots of 65MMA, 65EMA and 65BMA showed a similar release pattern of PDGF-AB with a peak at 8 h of lysis. Overall 65MMA led to a significantly higher PDGF-AB level at 1 h ($p \leq 0.001$) and 4 h ($p \leq 0.05$) after lysis (**Figure 6c**). Unlike PDGF-AB, the release of TGF-β1 gradually increased over the course of lysis (**Figure 6d**). With a similar pattern of release, 65BMA led to a significantly higher TGF-β1 level than 65EMA at 1 h and 4 h of lysis ($p \leq 0.05$) (**Figure 6d**). In summary, both PDGF-AB and TGF-β1 were released at higher amounts during clot formation than during clot lysis.

4. Discussion

In this study we investigated whether blood response and blood clot formation could be modulated on the coating surface of artificial bone implants through surface chemical functionalities and their compositions. Our strategy of presenting surface functionalities –COOH/–CH_3, –CH_2CH_3 or –$(CH_2)_3CH_3$) at different compositions was accomplished by varying AA/MMA, EMA or BMA at

different mole fractions in forming the materials. Our results showed that the inner surface of incubation vial was modified effectively by the material coating. Such a surface coating is a common and efficient way to modify implants having complex geometries without altering the bulk properties[30]. We found that an increase in AA proportion generally increased the surface content of –COOH groups but the content of –COOH groups was lower than the expected AA fraction. Similar observations were found in other studies and might be attributed to different degrees of copolymerisation in related to monomer reactivity ratios[31], polymer chain mobilities of PAA and poly(alkyl methacrylates) in subsurface layer which is beyond sampling depth (<10 nm) of XPS, as well as reorientation of hydrophilic functional group to avoid air exposure[32].

Our results demonstrated that surface hydrophobicity of coated surfaces correlates well with the chemical compositions, as in accordance to the literature[33, 34]. At relatively the same –COOH ratios, surfaces presenting –$(CH_2)_3CH_3$) groups exhibited a higher hydrophobicity than –CH_3 and –CH_2CH_3 groups whereas the latter two did not differ significantly. This suggests that the difference in one-carbon length between –CH_3 and –CH_2CH_3 groups has limited impact on modulating surface hydrophobicity in the presence of –COOH groups. In fact, both the nature of functional groups and their relative compositions are the key factors in controlling surface hydrophobicity[35]. In contrast, there is no evident relationship between surface roughness and surface functional groups and their ratios.

It was showed that surface functional groups and their compositions strongly influence the rate of coagulation activation. Increasing –COOH ratios (from 33% to 40%) on surfaces with –COOH/–CH_3 and –CH_2CH_3 decrease the rate of the activation. This finding is surprising since the initiation of intrinsic pathway on –COOH/–CH_3 SAM surfaces has been shown to increase with increasing –COOH ratio[19, 36]. Previous studies also demonstrated that FXII activation of intrinsic pathway is directly dependent on the amount of negatively charged functional groups[37, 38]. Indeed, Sperling *et al*. [19]found that –COOH/–CH_3 SAM surfaces with less than 50% –COOH did not show FXIIa activity in plasma phase. Rather, these surfaces had a noticeable effect on activating FXII adsorbed

on the surfaces. In addition, activated platelets were reported to trigger FXII activation on their surfaces and induce FXIIa-mediated intrinsic activation [39, 40]. However, platelet adhesion and activation have been shown to decrease with increasing –COOH content on –COOH/–CH_3 surfaces[29,30]. Given that interplay between FXIIa initiation and activated platelets propagation is crucial for a substantial coagulation response; a decline of platelet-dependent amplification of coagulation may explain our finding of an alteration of the rate of activation at 30 min.

In addition, our results showed that the surface alkyl groups have specific effects on the rate of coagulation initiation. Regardless of varied –COOH ratios, the surfaces with –$(CH_2)_3CH_3$) groups induced a faster rate of activation than –CH_3 and –CH_2CH_3 groups, and that varying –COOH ratios on –$(CH_2)_3CH_3$) bearing surfaces was less likely to affect the kinetic of coagulation. Hydrophobic materials were generally found to increase adsorption and conformational change of fibrinogen, which is proposed to be mediated by the strong hydrophobic interaction between D-domain of fibrinogen and the substrate, leading to stronger platelet adhesion and activation when compared to hydrophilic materials[41]. These observations are in line with earlier finding that more hydrophobic –$(CH_2)_3CH_3$) groups on a polymer surface yielded the highest fibrinogen adsorption, platelet activation and faster rate of coagulation activation compared to –CH_3 and –OH groups[42]. Accordingly, the weak electrostatic force between αC-domain of fibrinogen and negatively charged –COOH groups may also explain the minor effect of varying –COOH ratios in the presence of –$(CH_2)_3CH_3$) groups on the kinetic of coagulation, unlike seen on –CH_3 and –CH_2CH_3 bearing surfaces. Interestingly, between two less hydrophobic –CH_3 and –CH_2CH_3 groups, the –CH_3 group displayed a specific activity in inducing a faster rate of coagulation initiation. As the surfaces with these two alkyl groups did not show a significant difference in water contact angles at the same –COOH ratios, this finding suggests that the surface hydrophobicity (surface free energy) is not the sole factor that governs blood coagulation response. Sivaraman *et al*. [43]convincingly demonstrated that –COOH and –OH SAMs with similar levels of surface hydrophilicity induced a significant difference in the degree of structural change of adsorbed fibrinogen and albumin. Since surface

hydrophobicity is actually determined by the surface chemical species, the characteristics of the surface functionalities would play a more significant role in modulating coagulation activation.

Analysis of complement activation showed that all material-coated surfaces remarkably reduced the response compared to uncoated surfaces, indicating these surfaces had a weaker immunogenic property. In addition, we found that the complement response followed an entirely similar pattern of surface-activated coagulation. The high interdependence between complement and coagulation activation on material surfaces confirms our whole blood incubation system allows free cross-talk between both cascades to take place as it is found *in vivo*[44, 45]. More importantly, our data show unambiguously that surface functional groups and their relative ratios have a synergistic effect on modulating the activation of both cascades. The complement response on material surfaces was significantly reduced with the alkyl length in the order: $–(CH_2)_3CH_3$ > $–CH_3$ > $–CH_2CH_3$. Berglin *et al*. [20]suggested that complement activation is reduced with increased alkyl chain length of poly (alkyl methacrylates) ranged from 4 to 18 carbons. However, similar to our findings, they also found that PMMA with $–CH_3$ induces slightly less activation than PIBMA (poly (isobutyl methacrylate) with $–(CH_2)_3CH_3$, of which the complement activity did not differ from that of PBMA.

Examination of resultant blood clots showed that the material-coated surface modulated the fibrin architecture resulting in a thicker fibre at denser network at the clot exterior when compared to uncoated glass surfaces. The elevated levels of prothrombin F1+2 on uncoated glass and 55BMA surfaces produced clots with much thinner fibres when compared to material-coated surfaces and BMA surfaces, respectively. These findings are consistent with the work of Wolberg *et al*. [46]in which elevated prothrombin level triggers the formation of thinner fibrin due to increased initial rate, peak and total amount of thrombin generation. In addition, the clot interior showed dramatic changes in fibrin architectures from the exterior for all surfaces in which fibrin were thicker and at very loose network. Moreover, we found a consistent trend on fibrin density at the clot exterior and interior on surfaces containing same –COOH ratio but different alkyl groups. This indicates that the

surface functionalities and relative ratios have a specific influence on fibrin structuredensity throughout the clots.

To verify *in vivo* stability of the altered clot structure which is important for physical support at the injured sites and subsequent new bone ingrowth, we measured the rate of clot lysis using a suspended clot system. Our results demonstrated that all material-coated surfaces led to a significantly slower fibrinolysis in the first hour of lysis compared to the uncoated glass surfaces. This slower onset of fibrinolysis is in good agreement with the tight network and thicker fibrin observed on the clot exterior on coated surfaces, in accordance with literatures which indicated that fibrinolysis occurs predominantly faster on loose network and thinner fibrin[47].

To assess biological function of the altered clots for enhancing bone regeneration, we measured the clot releases of PDGF-AB and TGF-β1. It has been well documented that various growth factors are expressed in different phases of bone healing[48]. In particular, the initiation of bone regeneration is suggested to begin with the release of PDGF-AB and TGF-β1 after a clot is formed[49]. PDGF-AB is most abundant in platelet α-granules and is known to support chemotaxis and proliferation of fibroblasts, smooth muscle cells as well as endothelial cells, resulting in collagen synthesis and angiogenesis[50]. On the other hand, TGF-β1 is predominant in platelets, bone and cartilage. It is shown to serve as a mitogen for osteoblasts, fibroblasts and endothelial cells, as well as an inhibitor of osteoclasts[51, 52]. In addition, both PDGF-AB and TGF-β1 are chemotactic for inflammatory cells such as neutrophils, monocytes or macrophages, which establishes a positive feedback loop of growth factors within the injured bone[53]. In view of their function in supporting bone healing, we evaluated the potentials of modifications in fibrin structure and fibrin structure-dependent fibrinolysis on affecting the release of these growth factors from the intact and degrading clots.

Altogether, this work opens the new scope of blood clots generated on various surface functionalities for treating severe bone injuries. Our studies on the effect of surface chemistry on blood clots were initiated based on the notion that the normal mechanism of bone healing could be useful for enhancing the healing microenvironment in the presence of synthetic bone implants.

5. Conclusions

To our best knowledge, this is the first study which provides a comprehensive picture of how surface functional groups and their concentrations considerably modulate blood cascade activation in the context of whole blood clot formation; subsequent fibrin architecture, susceptibility to fibrinolysis and release of growth factors. The knowledge generated herein would allow a prior prediction of the whole blood response directly from the material formulation. These results explore the future potential of applying blood clot regulation by various material coatings to improve the efficacy of synthetic bone grafts.

Acknowledgements

We thank Dr Barry Wood of UQ for his support with X-ray photoelectron microscopy and Associate Professor Nunzio Motta for assisting with atomic force microscopy. The financial support from IHBI and the Queensland University of Technology is also gratefully acknowledged.

Legends:

Figure 1. XPS survey spectra of a) uncoated glass, b) PAA, c) PBMA, and d) 45BMA (45% AA/BMA) coated surfaces. XPS C1s spectra of e) PAA, f) PMMA, and g) 45MMA coated surfaces.

Figure 2. The serum levels of a) prothrombin F1+2, b) C5a-desArg, after whole blood incubation with material-coated surfaces relative to the uncoated glass surfaces (%). Plasma levels served as baseline. Data was presented as mean of six replicates of each surface with SD. * $p \leq 0.001$

Figure 3. Scanning electron microscopy analysis of whole blood clot structures formed on 45BMA, 55BMA, 65BMA and uncoated glass surfaces. Micrographs of the edge of clots (top panel; a-d) and the centre of clots (bottom panel; e–h), scale bar represents 20 μm. Comparison of fibrin thickness (diameter; nm) i) at the edge; j) at the centre of clots. Comparison of fibrin density (fibre number per 40 μm^2) k) at the edge; l) at the centre of clots. Data of fibrin thickness was presented as mean of at least 40 fibrin fibres measured at random field while data of fibrin density was presented as mean of fibre numbers quantified in at least 20 random areas of 40 μm^2 at the edge and at the centre of the clots of each surface with SD.* $p \leq 0.001$.

Figure 4. Scanning electron microscopy analysis of structure of clots formed on 65MMA, 65EMA, 65BMA and uncoated glass surfaces. SEM micrographs of the edge of clot (top panel; a-d) and the centre of clot (bottom panel; e–h), scale bar represents 20 μm. Comparison of fibrin diameter (nm) i) at the edge; j) at the centre of clots. Comparison of fibrin density (fibre number per 40 μm^2) k) at the edge; l) at the centre of clots. Data of fibrin thickness was presented as mean of at least 40 fibrin fibres measured at random field while data of fibrin density was presented as mean of fibre numbers quantified in at least 20 random areas of 40 μm^2 at the edge and at the centre of the clots of each surface with SD.* $p \leq 0.001$.

554

555 **Figure 5.** Release of D-dimer during clot lysis. The D-dimer levels of clots on BMA surfaces a)
556 after 1 h compared to uncoated glass surfaces, and c) over 24 h of lysis. The D-dimer levels of clots
557 on 65MMA, 65EMA and 65BMA surfaces b) after 1 h compared to uncoated glass surfaces, and d)
558 over 24 h of lysis. e) The D-dimer levels over 24 h-lysis period of uncoated glass surfaces and
559 relative control clots subject to PBS only.

560

561 **Figrue 6.** The serum levels of a) PDGF-AB and b) TGF-β1 after 2 h of whole blood incubation
562 with 65MMA, 65EMA and 65BMA surfaces compared to the uncoated glass surfaces and the
563 plasma baseline. *In vitro* releases of c) PDGF-AB and d) TGF-β1 during lysis of clots formed on
564 65MMA, 65EMA and 65BMA surfaces. Data was presented as mean of triplicates of each surface
565 with SD.* $p \leq 0.001$ ** $p \leq 0.05$

566

567 **Table 1.** Ratio of –COOH groups measured on surface coatings (X_{COOH} coating) compared to mole
568 fraction of –COOH group-containing AA (X_{COOH} material) composed with MMA, EMA or BMA.
569 Data were presented as the average value of three measurements.

570

571 **Table 2.** Advancing contact angles of surfaces coated with materials composed of varied mole
572 fraction of AA (X_{COOH} material) with MMA, EMA or BMA. Measurements were reported as the
573 average value of contact angles of at least six data points.

574

575

Reference

1. Y. Xiao, H. Qian, W. G. Young and P. M. Bartold, *Tissue Eng*, 2003, 9, 1167-1177.
2. P. M. Bartold, Y. Xiao, S. P. Lyngstaadas, M. L. Paine and M. L. Snead, *Periodontology 2000*, 2006, 41, 123-135.
3. D. Logeart-Avramoglou, F. Anagnostou, R. Bizios and H. Petite, *J Cell Mol Med*, 2005, 9, 72-84.
4. I. Schleicher, A. Parker, D. Leavesley, R. Crawford, Z. Upton and Y. Xiao, *Tissue engineering*, 2005, 11, 1688-1698.
5. N. E. Carlson and R. B. Roach, Jr., *J Am Dent Assoc*, 2002, 133, 1383-1386.
6. Y. Roussy, M. P. Bertrand Duchesne and G. Gagnon, *Clin Oral Implants Res*, 2007, 18, 639-648.
7. J. van den Dolder, R. Mooren, A. P. Vloon, P. J. Stoelinga and J. A. Jansen, *Tissue Eng*, 2006, 12, 3067-3073.
8. G. Weibrich, T. Hansen, W. Kleis, R. Buch and W. E. Hitzler, *Bone*, 2004, 34, 665-671.
9. M. E. Carr, Jr., E. J. Martin and S. L. Carr, *Blood Coagul Fibrinolysis*, 2002, 13, 193-197.
10. A. S. Wolberg, *Blood Rev*, 2007, 21, 131-142.
11. J. P. Collet, H. Shuman, R. E. Ledger, S. Lee and J. W. Weisel, *Proc Natl Acad Sci U S A*, 2005, 102, 9133-9137.
12. W. Liu, L. M. Jawerth, E. A. Sparks, M. R. Falvo, R. R. Hantgan, R. Superfine, S. T. Lord and M. Guthold, *Science*, 2006, 313, 634.
13. D. A. Gabriel, K. Muga and E. M. Boothroyd, *J Biol Chem*, 1992, 267, 24259-24263.
14. J. P. Collet, J. Soria, M. Mirshahi, M. Hirsch, F. B. Dagonnet, J. Caen and C. Soria, *Blood*, 1993, 82, 2462-2469.
15. J. D. Mills, R. A. Ariens, M. W. Mansfield and P. J. Grant, *Circulation*, 2002, 106, 1938-1942.
16. J. E. Davies, *J Dent Educ*, 2003, 67, 932-949.
17. W. E. Oprea, J. M. Karp, M. M. Hosseini and J. E. Davies, *J Craniofac Surg*, 2003, 14, 292-300.
18. M. B. Gorbet and M. V. Sefton, *Biomaterials*, 2004, 25, 5681-5703.
19. C. Sperling, M. Fischer, M. F. Maitz and C. Werner, *Biomaterials*, 2009, 30, 4447-4456.
20. M. Berglin, M. Andersson, A. Sellborn and H. Elwing, *Biomaterials*, 2004, 25, 4581-4590.
21. H. B. Lee, G. Khang and J. H. Lee, *Biomaterials*, 2007, 3-1 - 3-21.
22. M. J. Butler and M. V. Sefton, *J. Biomed. Mater. Res., Part A*, 2007, 82, 265-273.
23. G. A. Hutcheon, C. Messiou, R. M. Wyre, M. C. Davies and S. Downes, *Biomaterials*, 2001, 22, 667-676.
24. X. Yan and R. A. Gemeinhart, *J. Controlled Release*, 2005, 106, 198-208.
25. S. Fujishita, C. Inaba, T. Ishisaka, M. Gemmei-Ide and H. Kitano, *Colloids Surf B Biointerfaces*, 2009, 74, 45-50.
26. C. Sperling, R. B. Schweiss, U. Streller and C. Werner, *Biomaterials*, 2005, 26, 6547-6557.
27. A. Undas, K. Szuldrzynski, E. Stepien, J. Zalewski, J. Godlewski, W. Tracz, M. Pasowicz and K. Zmudka, *Atherosclerosis*, 2008, 196, 551-557.
28. P. T. Onundarson, C. W. Francis and V. J. Marder, *J Lab Clin Med*, 1992, 120, 120-128.
29. S. Takemoto, T. Yamamoto, K. Tsuru, S. Hayakawa, A. Osaka and S. Takashima, *Biomaterials*, 2004, 25, 3485-3492.
30. Z. Ma, Z. Mao and C. Gao, *Colloids Surf B Biointerfaces*, 2007, 60, 137-157.
31. K. I. Ekpenyong, *J Chem Educ*, 1985, 62, 173-174.
32. K. I. Ekpenyong, *Journal of Chemical Education*, 1985, 62, 173-174.
33. C. Ukiwe, A. Mansouri and D. Y. Kwok, *J Colloid Interf Sci*, 2005, 285, 760-768.
34. J. N. Lai, B. Sunderland, J. M. Xue, S. Yan, W. J. Zhao, M. Folkard, B. D. Michael and Y. G. Wang, *Appl Surf Sci*, 2006, 252, 3375-3379.

35. M. Y. Tsai, Y. T. Sun and J. C. Lin, *J Colloid Interf Sci*, 2007, 308, 474-484.
36. M. Fischer, C. Sperling and C. Werner, *J Mater Sci-Mater M*, 2010, 21, 931-937.
37. R. Zhuo, C. A. Siedlecki and E. A. Vogler, *Biomaterials*, 2006, 27, 4325-4332.
38. X. Y. Chen, J. Wang, Z. Paszti, F. L. Wang, J. N. Schrauben, V. V. Tarabara, A. H. Schmaier and Z. Chen, *Anal Bioanal Chem*, 2007, 388, 65-72.
39. P. E. van der Meijden and J. W. Heemskerk, *Expert Rev. Hematol.*, 2010, 3, 269-272.
40. J. Back, J. Sanchez, G. Elgue, K. N. Ekdahl and B. Nilsson, *Biochem. Biophys. Res. Commun.*, 2010, 391, 11-17.
41. H. Nygren, *Colloid Surface B*, 1996, 6, 329-333.
42. C. Sperling, M. F. Maitz, S. Talkenberger, M. F. Gouzy, T. Groth and C. Werner, *Biomaterials*, 2007, 28, 3617-3625.
43. B. Sivaraman, K. P. Fears and R. A. Latour, *Langmuir*, 2009, 25, 3050-3056.
44. M. M. Markiewski, B. Nilsson, K. N. Ekdahl, T. E. Mollnes and J. D. Lambris, *Trends Immunol*, 2007, 28, 184-192.
45. E. I. B. Peerschke, W. Yin and B. Ghebrehiwet, *Adv Exp Med Biol*, 2008, 632, 81-91.
46. A. S. Wolberg, D. M. Monroe, H. R. Roberts and M. Hoffman, *Blood*, 2003, 101, 3008-3013.
47. J. L. Mullin, S. E. Norfolk, J. W. Weisel and S. T. Lord, *Ann N Y Acad Sci*, 2001, 936, 331-334.
48. K. J. Cross and T. A. Mustoe, *Surg Clin North Am*, 2003, 83, 531-545, vi.
49. A. F. Kells, S. R. Coats, H. S. Schwartz and R. L. Hoover, *Connect Tissue Res*, 1995, 31, 117-124.
50. J. Andrae, R. Gallini and C. Betsholtz, *Genes Dev*, 2008, 22, 1276-1312.
51. H. Zhang, M. S. Aronow and G. A. Gronowicz, *J Biomed Mater Res A*, 2005, 75, 98-105.
52. M. Bosetti, F. Boccafoschi, M. Leigheb and M. F. Cannas, *Biomol Eng*, 2007, 24, 613-618.
53. G. S. Ashcroft, *Microbes Infect*, 1999, 1, 1275-1282.

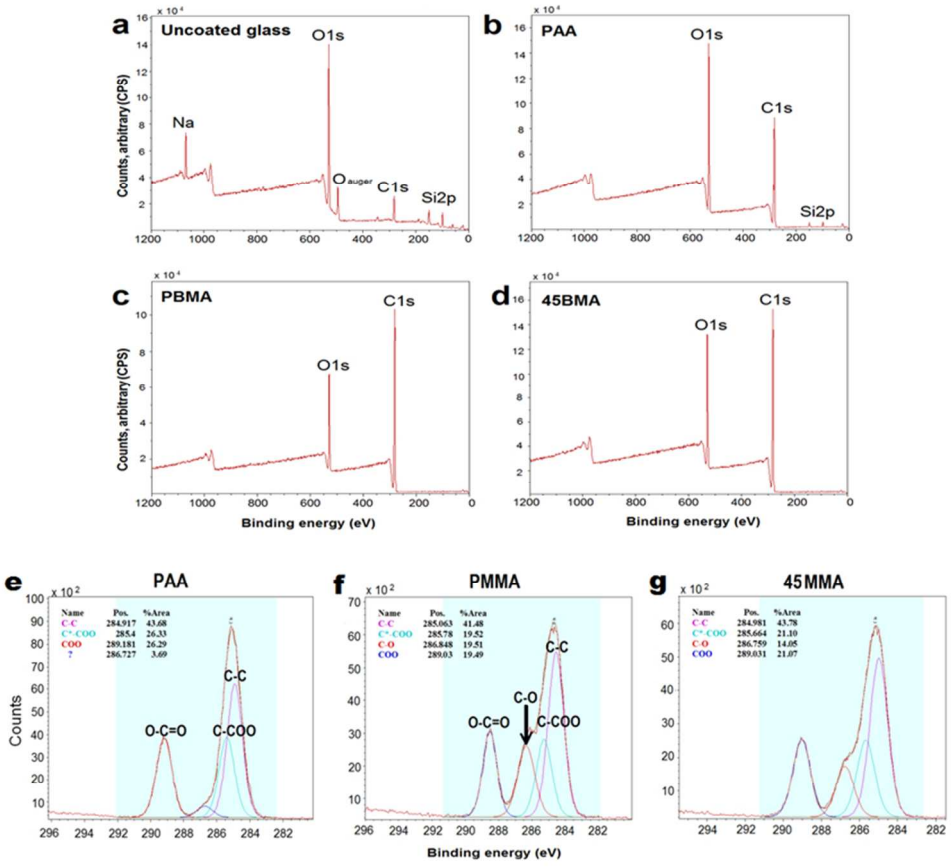

Figure 1. XPS survey spectra of a) uncoated glass, b) PAA, c) PBMA, and d) 45BMA (45% AA/BMA) coated surfaces. XPS C1s spectra of e) PAA, f) PMMA, and g) 45MMA coated surfaces.
150x134mm (150 x 150 DPI)

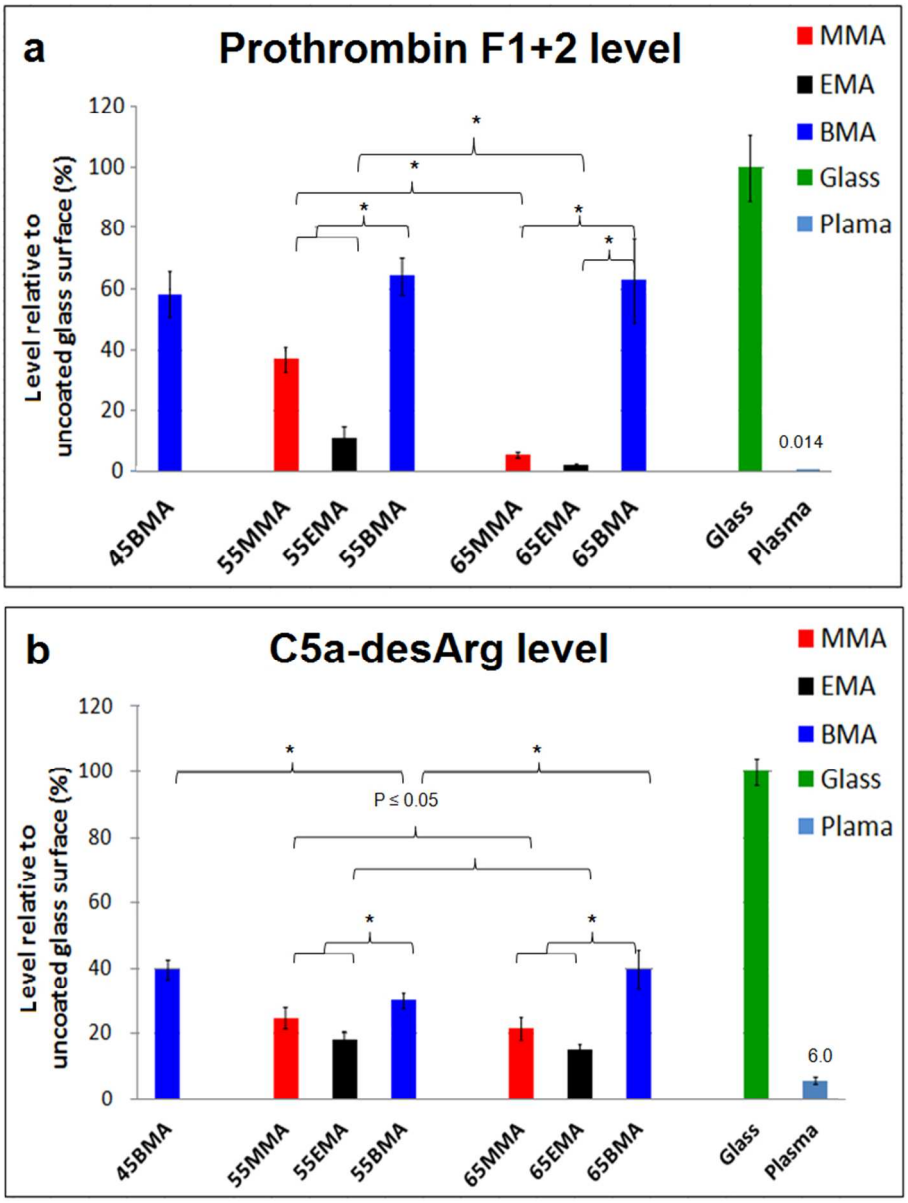

Figure 2. The serum levels of a) prothrombin F1+2, b) C5a-desArg, after whole blood incubation with material-coated surfaces relative to the uncoated glass surfaces (%). Plasma levels served as baseline. Data was presented as mean of six replicates of each surface with SD. * $p \leq 0.001$
213x282mm (96 x 96 DPI)

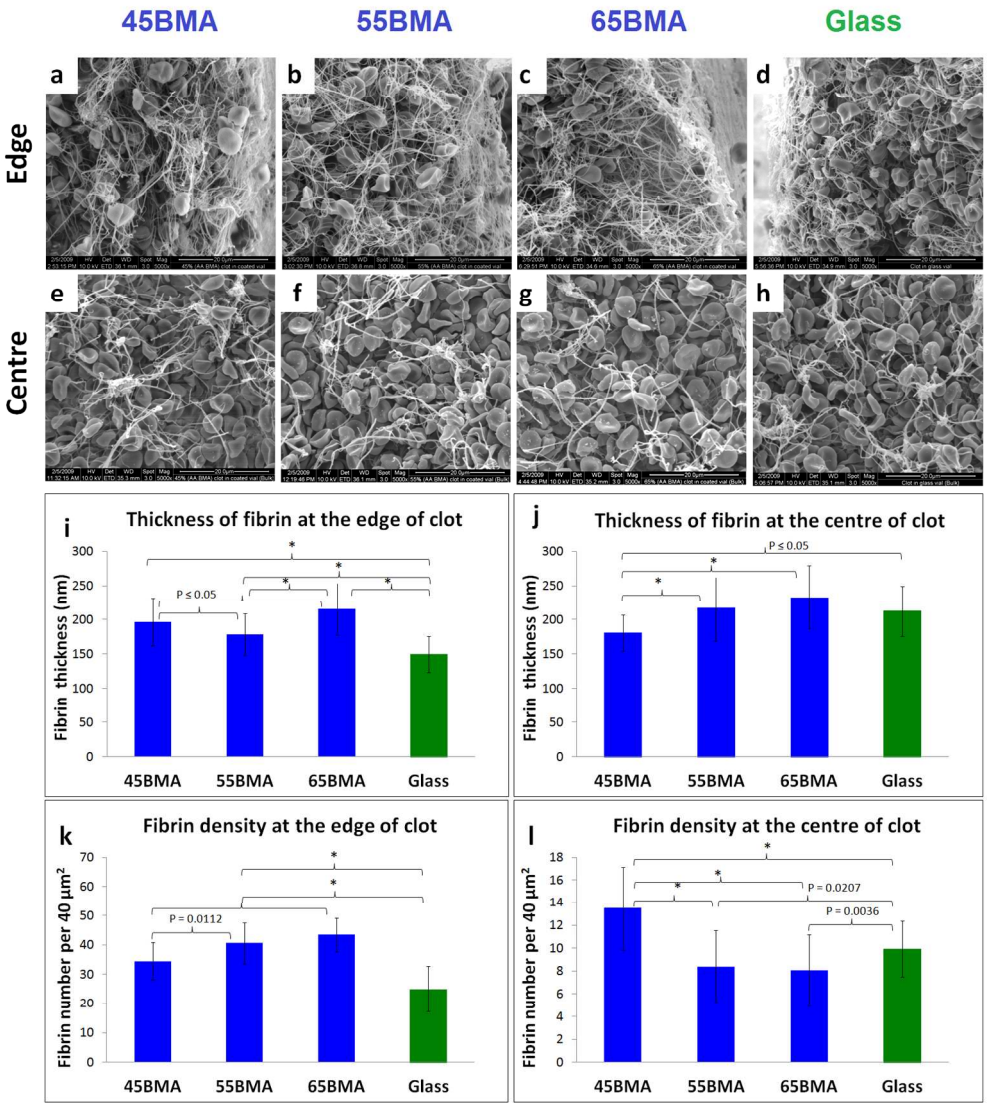

Figure 3. Scanning electron microscopy analysis of whole blood clot structures formed on 45BMA, 55BMA, 65BMA and uncoated glass surfaces. Micrographs of the edge of clots (top panel; a-d) and the centre of clots (bottom panel; e–h), scale bar represents 20 µm. Comparison of fibrin thickness (diameter; nm) i) at the edge; j) at the centre of clots. Comparison of fibrin density (fibre number per 40 µm2) k) at the edge; l) at the centre of clots. Data of fibrin thickness was presented as mean of at least 40 fibrin fibres measured at random field while data of fibrin density was presented as mean of fibre numbers quantified in at least 20 random areas of 40 µm2 at the edge and at the centre of the clots of each surface with SD.* p ≤ 0.001.
448x497mm (96 x 96 DPI)

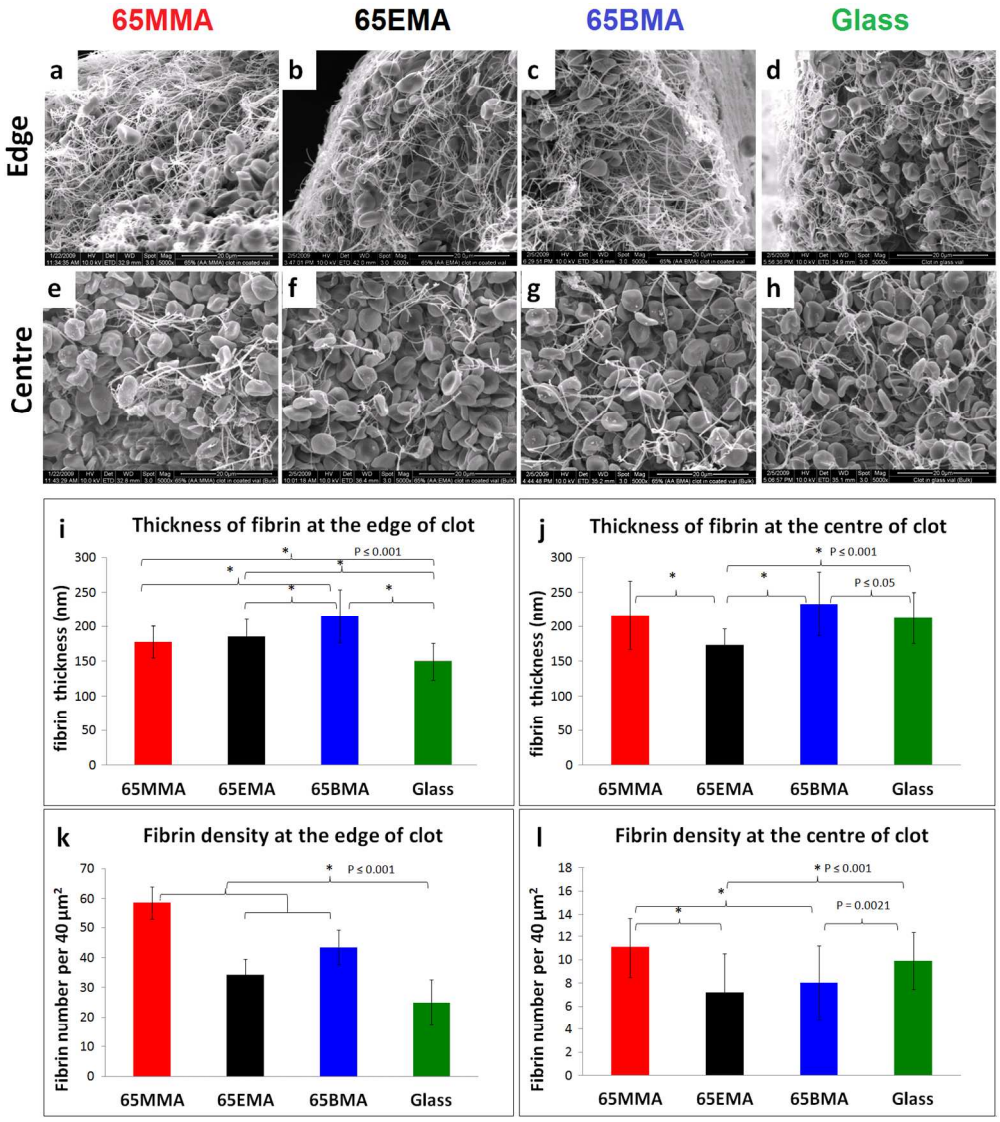

Figure 4. Scanning electron microscopy analysis of structure of clots formed on 65MMA, 65EMA, 65BMA and uncoated glass surfaces. SEM micrographs of the edge of clot (top panel; a-d) and the centre of clot (bottom panel; e–h), scale bar represents 20 µm. Comparison of fibrin diameter (nm) i) at the edge; j) at the centre of clots. Comparison of fibrin density (fibre number per 40 µm2) k) at the edge; l) at the centre of clots. Data of fibrin thickness was presented as mean of at least 40 fibrin fibres measured at random field while data of fibrin density was presented as mean of fibre numbers quantified in at least 20 random areas of 40 µm2 at the edge and at the centre of the clots of each surface with SD.* p ≤ 0.001.
440x493mm (96 x 96 DPI)

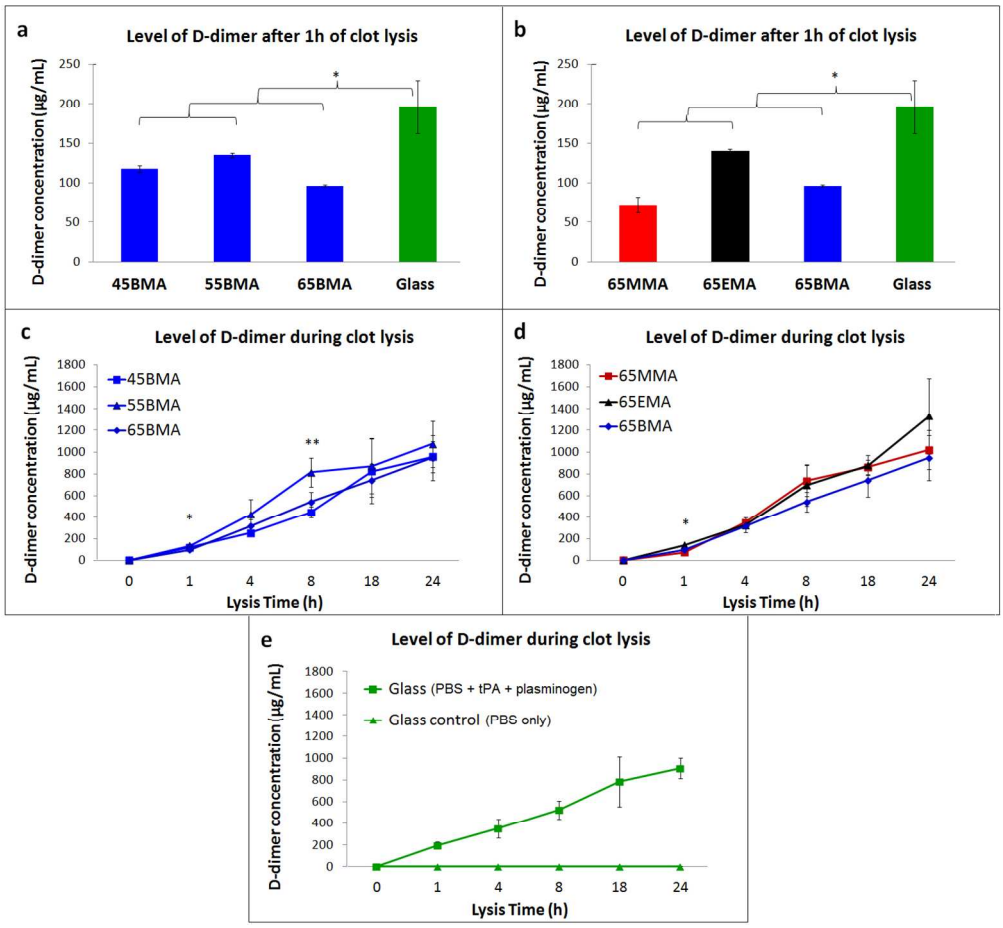

Figure 5. Release of D-dimer during clot lysis. The D-dimer levels of clots on BMA surfaces a) after 1 h compared to uncoated glass surfaces, and c) over 24 h of lysis. The D-dimer levels of clots on 65MMA, 65EMA and 65BMA surfaces b) after 1 h compared to uncoated glass surfaces, and d) over 24 h of lysis. e) The D-dimer levels over 24 h-lysis period of uncoated glass surfaces and relative control clots subject to PBS only.
403x370mm (96 x 96 DPI)

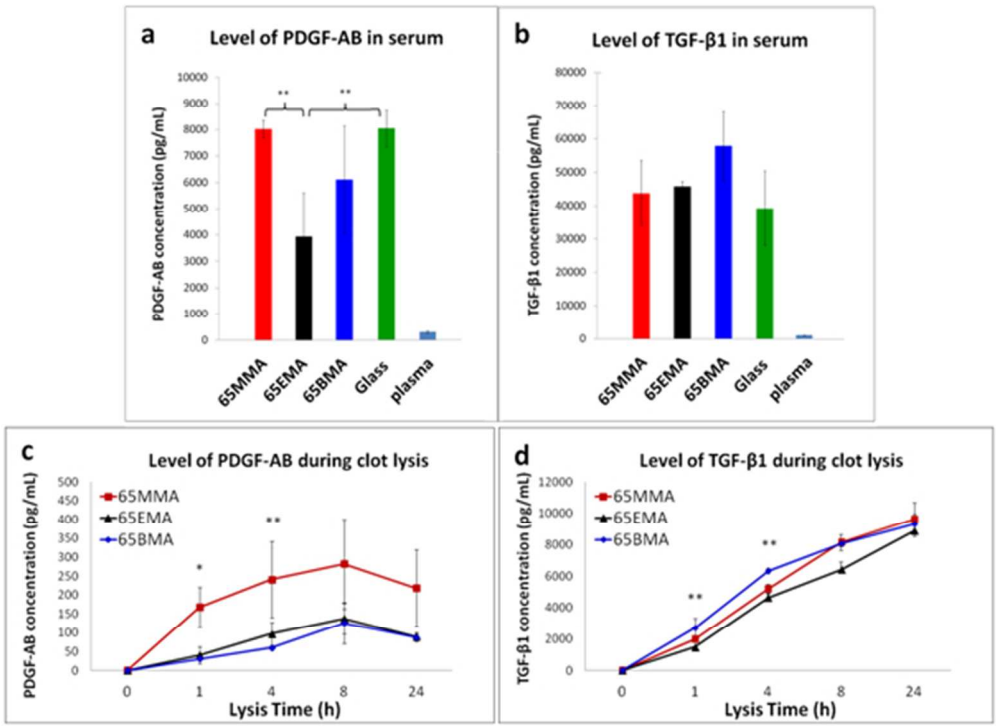

Figrue 6. The serum levels of a) PDGF-AB and b) TGF-β1 after 2 h of whole blood incubation with 65MMA, 65EMA and 65BMA surfaces compared to the uncoated glass surfaces and the plasma baseline. In vitro releases of c) PDGF-AB and d) TGF-β1 during lysis of clots formed on 65MMA, 65EMA and 65BMA surfaces. Data was presented as mean of triplicates of each surface with SD.* $p \leq 0.001$ ** $p \leq 0.05$
160x116mm (96 x 96 DPI)

Table 1: The surface ratios of –COOH/–CH_3, –CH_2CH_3 or –$(CH_2)_3CH_3$

X_{COOH} Materials	X_{COOH} Coating (MMA)	X_{COOH} Coating (EMA)	X_{COOH} Coating (BMA)
0	0	0	0
0.25	0.20	0.17	0.13
0.45	0.34	0.33	0.25
0.55	0.34	0.32	0.33
0.65	0.41	0.39	0.41

Ratio of –COOH groups measured on surface coatings (X_{COOH} coating) compared to mole fraction of –COOH group-containing AA (X_{COOH} material) composed with MMA, EMA or BMA. Data were presented as the average value of three measurements.

Table 2: The advancing contact angle value of coated substrate

X_{COOH} copolymer	MMA	EMA	BMA
0	77.6 ± 3.1	82.9 ± 1.0	91.8 ± 4.4
0.25	74.3 ± 4.3	77.1 ± 2.2	88.3 ± 1.4
0.45	72.4 ± 4.6	74.9 ± 2.6	86.7 ± 1.0
0.55	73.4 ± 8.6	75.1 ± 1.7	84.4 ± 2.3
0.65	71.0 ± 2.7	73.7 ± 3.4	81.1 ± 2.4

Advancing contact angles of surfaces coated with materials composed of varied mole fraction of acrylic acid and alkyl methacrylates. Measurements were reported as the average value of contact angles of at least six data points.